Molecular Structure of Metallocene Catalyst $Cp^{tt}{}_2ZrCl_2$ and Structural Analysis of PE Catalyzed by $Cp^{tt}{}_2ZrCl_2$

Xiao-Yan Yu,[1] Qing-Xin Zhang,[1] Guo-Xin Jin,[1,2] Ning-Hai Hu[1]

[1]*State Key Laboratory of Polymer Physics and Chemistry, Changchun Institute of Applied Chemistry, Chinese Academy of Sciences, Changchun 130022, People's Republic of China*
[2]*Chemistry Department, Fudan University, Shanghai 200433, People's Republic of China*

Received 13 February 2002; accepted 3 September 2004
DOI 10.1002/app.21377
Published online 27 January 2005 in Wiley InterScience (www.interscience.wiley.com).

ABSTRACT: $Cp^{tt}{}_2ZrCl_2$ ($Cp^{tt} = \eta^5-{}^tBu_2C_5H_3$) was synthesized by the reaction of $LiCp^{tt}$ with $ZrCl_4$ and characterized by X-ray crystallographic studies. It was used as catalyst for ethylene polymerization. Structural analysis was carried out on the polyethylene (PE) catalyzed by $Cp^{tt}{}_2ZrCl_2$ via wide-angle X-ray diffraction (WAXD) and small-angle X-ray scattering (SAXS). The degree of crystallinity ($W_{c,x}$) was calculated by WAXD. The semiaxises of the particles (*a*, *a*, *b*) of PE were determined by SAXS and it could be found that the crystalline particles of PE are mainly rod shaped determined by the characteristic function v_0 (*r*). The radius of gyration R_g, crystalline thickness L_c, the thickness of noncrystalline region L_a, long period *L*, electron-density difference between the crystalline and noncrystalline regions $\eta_c - \eta_a$, and the invariant *Q* are determined by SAXS. The results also indicate that a transition zone exists between the traditional "two phases" with a clear dimension of 1.3 nm. © 2005 Wiley Periodicals, Inc. J Appl Polym Sci 96: 169–175, 2005

Key words: crystal structure; metallocene catalyst; polyethylene; WAXD; SAXS

INTRODUCTION

As highly effective catalysts for olefin polymerization, metallocene complexes Cp_2MCl_2 ($Cp = \eta^5$-C_5H_5, M = Ti, Zr, Hf) have attracted a great deal of interest during past two decades.[1] Usually the substitutes on the cyclopentadienyl cycles would make some differences in catalytic properties and have more or less influence on the structures and properties of the polymer products. The use of the cyclopentadienyl ligand with one or two *tert*-butyl substitutes is postulated to generate a fairly considerable steric effect on the complex structure and, therefore, the activity for the catalysis of ethylene polymerization.[2,3] Although there are many reports in this area, detailed work on both the crystal structure of the catalyst containing 1,3-di-*tert*-butylcyclopentadienes and the corresponding activity for the catalysis of ethylene polymerization is still limited.[4]

WAXD is a powerful method to study the crystal structure of polymer. SAXS can be used to characterize the parameters of particles over a length range larger than the usual interatomic distances. On the basis of a lattice theory, Flory et al.[5] suggested that an interphase region might exist in the lamellae between the crystalline and noncrystalline region of semicrystalline polymers, the properties of which differ from those of a truly noncrystalline region. Hahn et al.[6] pointed out that the formation of an interphase region was an intrinsic property of the lamellae within crystalline regions and that such an interphase region must influence the structural and dynamical properties of the polymer. The thickness of the interphase region was predicted to be 1–2 nm.[5] Comparing the thickness of the interphase region with the thickness of the crystal lamellae indicated that this value is reasonable. Instead of the traditional two-phase model, a three-phase model has been proposed to explain these results by means of SAXS.

In this paper, metallocene complex $Cp^{tt}{}_2ZrCl_2$ ($Cp^{tt} = \eta^5-{}^tBu_2C_5H_3$) was synthesized and characterized crystallographically. It can be used as a catalyst for ethylene polymerization in the presence of cocatalyst MMAO. Detailed structural analysis of the PE catalyzed by it was carried out by SAXS.

EXPERIMENTAL

Synthesis of $Cp^{tt}{}_2ZrCl_2$ and Catalysis of Ethylene Polymerization

$Cp^{tt}{}_2ZrCl_2$ was synthesized from the reactions of $LiCp^{tt}$ with $ZrCl_4$ under pure argon atmosphere according to the literature[4] and recrystallized from the

Correspondence to: G.-X. Jin (gxjin@fudan.edu.cn).
Contract grant sponsor: National Natural Science Foundation of China (29925101) and Special Founds for Major State Basic Research Projects (G1999064800).

TABLE I
Crystallographic Data for Complex $Cp^{tt}{}_2ZrCl_2$

Color	Light yellow
Habit	Block
Formula	$C_{26}H_{42}Cl_2Zr$
Formula weight	516.72
Cryst size (mm)	0.46 × 0.32 × 0.08
Cryst system	Monoclinic
Space group	Pn
a (Å)	12.874(5)
b (Å)	6.687(2)
c (Å)	16.137(4)
β (deg)	97.09(3)
V (Å)	1378.5(8)
Z	2
D_{calcd}, $(Mg/m)^3$	1.245
θ range (deg)	2.16–25.06
μ (mm^{-1})	0.602
Reflections collected	3381
Independent reflections	2763 (R_{int} = 0.0368)
R [$I > 2\sigma(I)$]	0.0538
R_w [$I > 2\sigma(I)$]	0.1484
No. of parameters	274
GOF on F^2	1.051

mixture solution of toluene/hexane at −30°C. One week later light yellow crystals were obtained from the solution. The crystals were resolved in toluene and used as catalyst for ethylene polymerization. To a well-stirred solution of ethylene in toluene (50 ml) with a flow of ethylene gas (atmosphere pressure), a solution of $Cp^{tt}{}_2ZrCl_2$ and a cocatalyst of modified methylalumoxane (MMAO) was added at 25°C. After 30 min, 200 ml of methanol and 1 ml of *conc.* HCl were added to the resulting mixture. The polymer obtained was collected by filtration and washed with methanol. The collected polymer was dried *in vacuo* at 80°C for 10 h. M values were determined by a GPC measurement at 135°C using polyethylene calibration.

Structure Solution and Refinement for $Cp^{tt}{}_2ZrCl_2$

For $Cp^{tt}{}_2ZrCl_2$, a single crystal suitable for X-ray was sealed into a glass capillary and mounted on a Siemens P4 diffractometer. All the determinations of unit cell and intensity data were performed with graphite monochromated Mo $K\alpha$ radiation (λ = 0.71073 Å). All the data were collected at room temperature using the ω scan technique. The structure was solved by the direct methods, expanded using Fourier techniques, and refined on F^2 by a full-matrix least-squares method. The nonhydrogen atoms were refined anisotropically and hydrogen atoms were included but not refined. All the calculations were carried out with a Siemens SHELXTL PLUS program. Details of crystal data are summarized in Table I.

WAXD

PE powders were hot pressed at 160°C for 5 min and then isothermally crystallized at 100°C for 4 h to form films with thickness of about 1 mm for WAXD and SAXS.

WAXD experiments were performed at room temperature using a Rigaku D/max 2500 V X-ray diffractometer in combination with an 18-kW rotating-anode generator operated at 40 kV and 200 mA, imaging plates, and curved graphite crystal filtered Cu $K\alpha_1$ radiation (λ = 0.15406 nm). WAXD data were collected from $2\theta = 10 \sim 60°$ with a step interval of 0.02°.

SAXS

SAXS experiments were carried out at room temperature using the Rigaku D/max 2500 V X-ray diffractometer operated at 40 kV and 200 mA with a four-slit collimation system. Data were collected from $2\theta = 0.07 \sim 3°$. The measured intensity was corrected for background scattering and absorption by the sample.

RESULTS AND DISCUSSION

Synthesis and Structural Characterization of $Cp^{tt}{}_2ZrCl_2$

The reaction between $ZrCl_4$ and $LiCp^{tt}$, which was prepared from the reaction of $Cp^{tt}H$ with ^nBuLi, afforded $Cp^{tt}{}_2ZrCl_2$. $Cp^{tt}{}_2ZrCl_2$ was isolated as light yellow crystals. The molecular structure of complex $Cp^{tt}{}_2ZrCl_2$ is presented in Figure 1, together with the atomic label. There are two $Cp^{tt}{}_2ZrCl_2$ molecules in the unit cell. In this complex, the zirconium atom is coordinated to two Cp^{tt} ligands and two chloride atoms. The two *tert*-butyl substitutes on the Cp^{tt} ligand are opposite to each other to avoid the bulky steric effect. The respective averaged Zr–C bond distances [C(11)– C(15) ring and C(21)–C(25) ring] are 2.55(2) and 2.54(2) Å, among those found in other analogous complexes.[4,7,8] The averaged C–C bond distances for the two Cp^{tt} rings are 1.42(3) and 1.40(3) Å, respectively. The distances between the zirconium atom and the two cents of the Cp^{tt} rings are 2.246 and 2.239 Å. The bond distances of Zr–Cl(1) and Zr–Cl(2) (2.465(5) and 2.428(4) Å) are not beyond the range for normal zirconium complexes. The two cents of Cp^{tt} rings and the two chlorides form a distorted tetrahedral sphere with the Cp^{tt}(1)–Zr–Cp^{tt}(2) angle of 129.6°. The chloride atoms are located at the *cis* position around the zirconium atom with the nearly perpendicular angle of 93.60(8)°.

Ethylene Polymerization Catalyzed by $Cp^{tt}{}_2ZrCl_2$

The polymerization was carried out *in situ* in toluene with the addition of modified methylalumoxane (MMAO) to $Cp^{tt}{}_2ZrCl_2$ in the presence of ethylene at atmosphere pressure. The catalyst afforded 81 g PE/(mmol cat · h) (T_m value 133.5°C) of activity with an

M_v value of 6×10^4, which is much lower than those of Cp_2ZrCl_2 and $Cp^t{}_2ZrCl_2$ ($Cp^t = \eta^5-$ $^tBuC_5H_4$).[4,9] Attachment of two *tert*-butyl groups, being sterically bulkier than a *tert*-butyl group, dramatically decreased polymerization activity and slightly decreased M_v. Probably, introduction of the two bulky *tert*-butyl groups to the cyclopentadienyl ring greatly lowered the possibility for providing vacants during the ethylene polymerization and thus dramatically decreased the polymerization activity.

Crystallinity Analysis

The WAXD pattern of catalyzed PE is shown in Figure 2 and the degree of crystallinity, $W_{c,x}$ is given by[10]

$$W_{c,x} = \frac{I_{110} + 1.42I_{200}}{I_{110} + 1.42I_{200} + 0.75I_a} \quad (1)$$

where I_{110}, I_{200}, and I_a are the integrating intensities of the (110) peak, (200) peak, and the noncrystalline regions, respectively. To determine the exact integrating intensities, a deconvolution procedure was performed, and the $W_{c,x}$ of PE was calculated to be 77.9% using eq. (1).

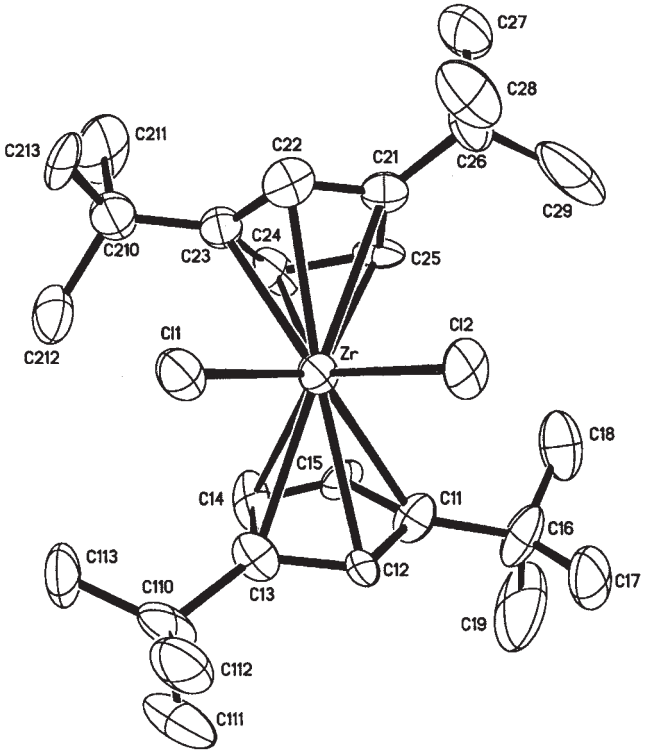

Figure 1 Molecular structure of complex $Cp^{tt}{}_2ZrCl_2$ (The hydrogen atoms are omitted for clarity). Selected bond distances (Å) and bond angles (°): Zr-C(11) 2.58(2); Zr-C(12) 2.63(2); Zr-C(13) 2.56(2); Zr-C(14) 2.48(2); Zr-C(15) 2.50(2); Zr-C(21) 2.64(2); Zr-C(22) 2.56(2); Zr-C(23) 2.56(2); Zr-C(24) 2.46(2); Zr-C(25) 2.46(2); Zr-Cl(1) 2.465(5); Zr-Cl(2) 2.428(4); Cl(1)-Zr-Cl(2) 93.60(8).

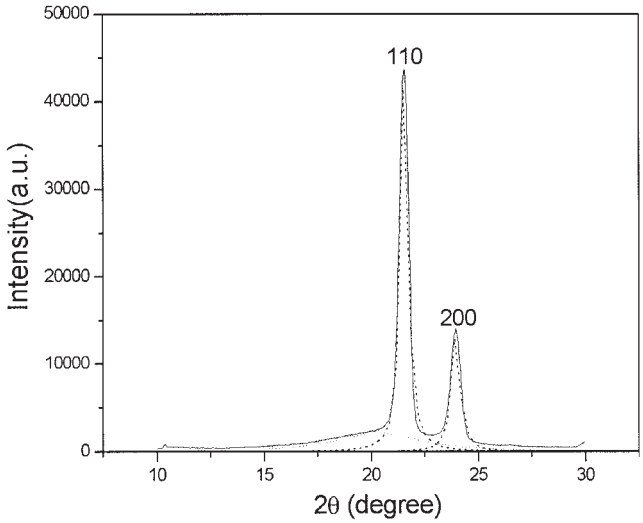

Figure 2 WAXD pattern of PE.

SAXS Analysis

SAXS reflects electron-density fluctuations within a sample over a length range larger than the usual interatomic distances. Semicrystalline PE, which consists of a simplified two-phase system of alternating crystalline domains and a noncrystalline matrix, could be assumed to be a system with fluctuating electron density, and it should scatter X-rays. The scattering capacity depends on the density difference between the crystalline and noncrystalline regions. The SAXS curve of PE is shown in Figure 3 and a deconvolution procedure was performed since experimental curve

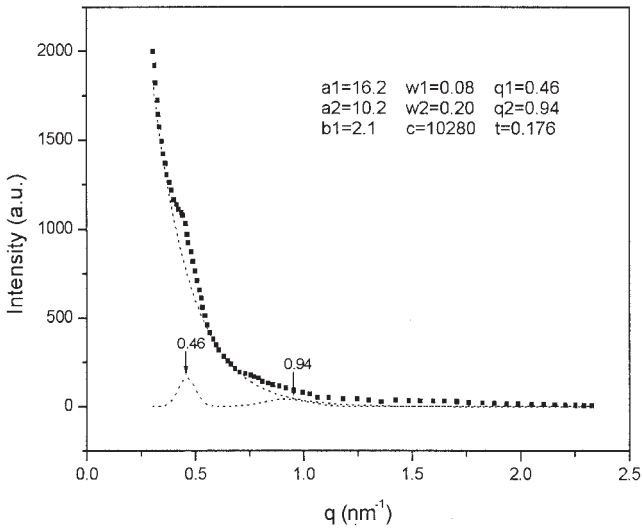

Figure 3 SAXS curve of PE.

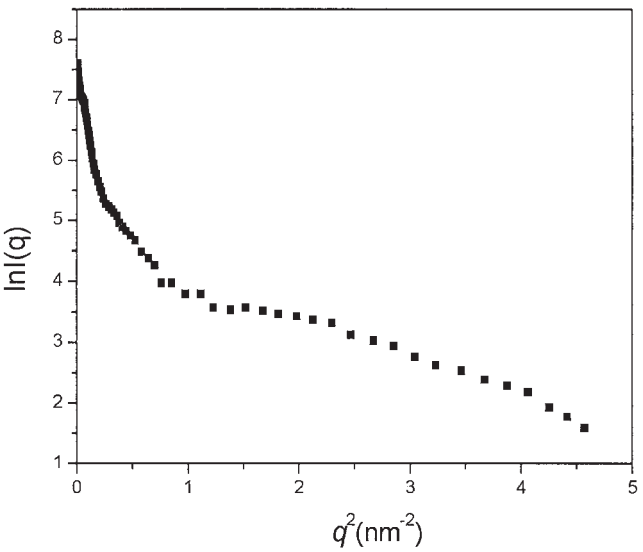

Figure 4 Plots of ln$I(q)$ vs. q^2 for PE.

can be expressed as the sum of the Gaussian function and the first-order exponential decay function:

$$I(q) = I_{\text{Gaussian}} + I_{\text{Guinier}} \tag{2}$$

$$I(q) = \sum_i \frac{a_i}{w_i\sqrt{\pi/2}} \exp\left[-\frac{2(q-q_i)^2}{w_i^2}\right] + b + c\exp\left[-\frac{q}{t}\right] \tag{3}$$

where a_i, b, c, t_i, and w_i are deconvolution parameters. The first-order exponential decay function was well fitted in PE. Bragg reflection can be obtained by the nonlinear fit on basis of eq. (3). PE shows two reflection peaks where the peak position ratios are almost 1 : 2, which indicates that these peaks are originated from the same long periodic structure of PE.

Radius of Gyration

Guinier and Fournet[11] and Wu and Speapan[12] have shown that the scattering intensity $I(q)$ of the polymer at small angle can be shown with the following equation:

$$I(q) \approx I_e N n^2 e^{-q^2 R_g^2/3} \tag{4}$$

where I_e is the scattering intensity of a electron, N is the number of all the irradiated particles, n is the electron number of one particle, $q = 4\pi \sin\theta/\lambda$, λ is the wavelength of X-ray, 2θ is the scattering angle, and R_g is the radius of gyration.

The logarithm form of eq. (4) is

$$\ln I(q) = \frac{R_g^2}{3}q^2 + \ln(I_e N n^2)$$

$$= Kq^2 + B \tag{5}$$

where $K = -R_g^2 3$ and $B = \ln(I_e N n^2)$. K is the slope, B is the intercept of $\ln I(q) \sim q^2$ curve, and $I_e N n^2$ is the intensity coefficient. The R_g and $I_e N n^2$ are given by

$$R_g = \sqrt{-3K} \tag{6}$$

$$I_e N n^2 = e^B \tag{7}$$

The ln$I(q) \sim q^2$ curve will be close to straight line within the small angle range for all the shapes of particles according to Guinier and Fournet.[11] This angle range is broader for the sphere particles system than the others, and it will decrease with the particles departuring from the spherical shape. Figure 4 shows the plot of ln$I(q) \sim q^2$ of PE. The radii of gyration R_g is obtained by eq. (6) and is shown in Table II.

Characteristic Function $v_0(r)$

The characteristic function v_0 (r) was introduced by Porod.[13,14] It has no intuitive connection with the form of the particle. v_0 (r) represents the probability that a point at a distance r in an arbitrary direction from a given point in the particle will itself also be in the particle, which could be written as[11,15]

$$v_0(r) = \frac{\frac{1}{r}\int_0^\infty qI(q)\sin(qr)dq}{\int_0^\infty q^2 I(q)dq} \tag{8}$$

The following four equations can be draw from eq. (8):[11]

$$v_0 < L_c > = 0 \tag{9}$$

TABLE II
Structural Parameters of the Solid State for PE

R_g (nm)	8.46
a (nm)	1.68
b (nm)	18.78
ω	11.18
$\bar{Q}$ (mol e cm^{-3})	5.9
$\bar{d}$ (nm)	8.4
L_c (nm)	9.8
L_a (nm)	2.7
d_{tr} (nm)	1.3
L (nm)	15.1

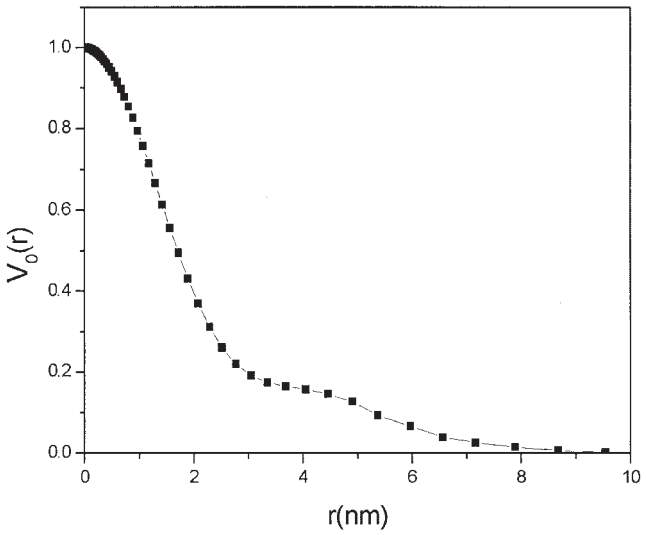

Figure 5 Plot of particle characteristic function $v_0(r)$.

$$\int_0^\infty v_0(r)dr = \frac{L_c}{2} \tag{10}$$

$$\int_0^\infty 4\pi r^2 v_0(r)dr = V_P \tag{11}$$

$$\left[\frac{dv_0(r)}{dr}\right]_{r\to 0} = -\frac{S}{4V_P} \tag{12}$$

where L_c is defined as the crystalline thickness, V_P is the volume of the particle, S is the surface area of the particle, and S/V_P is the specific surface area.

The characteristic function $v_0(r)$ of PE is shown in Figure 5. As we have discussed above, respectively, the crystalline thickness L_c and the specific surface area S_0/V_P can be obtained from the integral area of $v_0(r) \sim r$ curves and the slope of $v_0(r)$ curves when r approaches zero. To determine the semiaxises of the ellipsoid (a, a,b), the experimental curve $v_0(r)$ was compared with a series of simulative curves with the different values of axial ratio ω (= b/a) but the same radius of gyration, then the most analogous one must be obtained and the axial ratio can be determined. The semiaxises (a, a, b) can be calculated by

$$a = R_g\left(\frac{5}{\omega^2 + 2}\right)^{1/2} \tag{13}$$

$$b = \omega a \tag{14}$$

The specific surface area S/V_P, semiaxises (a, a, b) of the ellipsoid particles and the crystalline thickness L_c are calculated and shown in Table II.

One-Dimensional Electron Density Correlation Function $K(Z)$

If the variation of the electron density obeys a "linear model", i.e., the density variations mainly occur along the direction perpendicular to the lamellae, then, to describe the structural change of the system, we can use the 1D EDCF (one-dimensional electron density correlation function). The correlation function $K(Z)$ can be written as:[16,17]

$$K(Z) = \langle[\eta(Z') - \langle\eta\rangle][\eta(Z + Z') - \langle\eta\rangle]\rangle \tag{15}$$

where Z is the direction normal to lamellar stacks and the angular brackets indicate averaging over all coordinates Z' within a representative stack that will pass through an noncrystalline layer and a crystalline layer. The average electron density within the stack is called $\langle\eta\rangle$. $K(Z)$ can be obtained by Fourier transformation of the desmeared scattering intensities:

$$K(Z) = 4\pi\int_0^\infty s^2 I(s)\cos(2\pi sZ)ds \tag{16}$$

where $s = 2\sin\theta/\lambda$. As an example, the derived typical 1D EDCF $K(Z)$ of the lamellar structure for PE was demonstrated in Figure 6. From the well-known "self-correlation triangle" which reflects the electron-density correlation within a lamella, one can directly estimate various structural parameters of the solid state for PE by making use of some general properties of the correlation function. The invariant Q is the value of $K(Z)$ at $Z = 0$ which is also evaluated by extrapolating the straight-line section of the self-correlation region to the $K(Z)$ axis (see Fig. 6). Its physical meaning is the mean-square electron-density fluctuation, which could satisfactorily explain the changing tendency of the values of Q considering the variation of the elec-

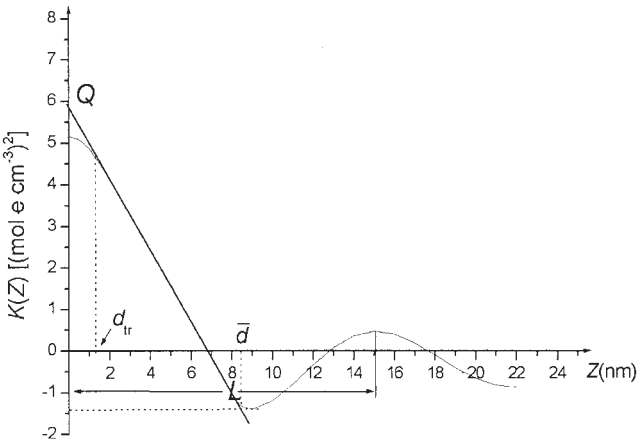

Figure 6 The curve of experimental correlation function $K(Z)$ obtained for PE.

tron-density difference with the annealing temperature. The long period L could be determined from the position of the first maximum in the correlation function. The average lamellar thickness $\bar{d}$ can be obtained by the cross point of the baseline with the sloping line of the "self-correlation triangle."

Buchanan et al.[18] proposed a two-phase model consisting of an infinite array of alternating crystalline and noncrystalline regions. From the traditional "ideal two-phase model," the self-correlation section of the SAXS curve was expected to be a straight line. As we employed a simplied two-phase model to analyze the SAXS data, the long period L should be expressed as $L = L_c + L_a$; here, L_c and L_a are the thickness of crystal and the noncrystalline regions, respectively. In fact, the deviation is usually observed in practical results, indicating that the boundaries between the crystalline and noncrystalline regions are not clear and sharp and there exists a transition zone[19–21] (interphase region) with finite width instead of a sharp jump in density. By the curvature of the straight-line segment in the central section of $K(Z)$, the thickness of the transition layer d_{tr} could be estimated. The most important difference between the two- and three-phase models is that the latter possesses a transition zone between the noncrystalline layer and the crystalline layer. According to Strobl and Schneider[16] the thickness of the transition zone d_{tr} can be directly derived from the curvature of $K(Z)$.

The thickness of the transition layer d_{tr} was given by the lower limit of the straight section in the self-correlation range. The noncrystalline thickness L_a can be calculated by

$$L = L_a + 2d_{tr} + L_c \tag{17}$$

The results of long period L, noncrystalline thickness L_a, invariant Q, average lamellar thickness $\bar{d}$, and thickness of transition layer d_{tr} are obtained and listed in Table II.

CONCLUSION

$Cp^{tt}{}_2ZrCl_2$ was synthesized and characterized crystallographically. It can be used as catalyst for ethylene polymerization. Structural analysis was carried out on the PE catalyzed by $Cp^{tt}{}_2ZrCl_2$ via SAXS. The degree of crystallinity ($W_{c,x}$) is calculated to be 77.9% by WAXD. The semiaxises of the particles (a, a, b) of PE were determined by SAXS and it could be found that the crystalline particles of PE were mainly rod shaped determined by the characteristic function. The radius of gyration R_g, crystalline thickness L_c, the thickness of noncrystalline region L_a, long period L, electron-density difference between the crystalline and noncrystalline regions $\eta_c - \eta_a$, and the invariant Q are determined by SAXS. The results also indicate that a transition zone exists between the traditional "two phases" with a clear dimension of 1.3 nm.

The authors thank the reviewers for their critical comments and good advice.

References

1. Alt, H. G.; Köppl, A. Chem Rev 2000, 100, 1205.
2. Jin, G.-X.; Liu, Y. Metallocene Catalysts for Olefin Polymerization; Chemical Industry Press: Beijing, 2000.
3. Zhou, G.-Y.; Jin, G.-X.; Huang, B.-T. Chem J Chinese Univ 2000, 21, 1489.
4. Cheng, Y.-X.; Yu, X.-Y.; Jin, G.-X.; Jia, H.-Q. Acta Polym Sinica 2001, 2, 139.
5. Flory, P. J.; Yoon, D. Y; Dill, K. A. Macromolecules 1984, 17, 862.
6. Hahn, B. R.; Herrmann-Schönherr, O.; Wendorff, J. H. Polymer 1987, 28, 201.
7. Howie, R. A.; McQuillan, G. P.; Thompson, D. W. J Organomet Chem 1984, 268, 149.
8. Jibril, I.; Abu-Orabi, S. T.; Klaib, S. A.; Zsolnai, L.; Huttner, G. J Organomet Chem 1994, 467, 189.
9. Matsui, S.; Fujita, T. Catalysis Today 2001, 66, 63.
10. Yin, J. H.; Mo, Z. S. Modern Polymer Physics; Sciences Press: Beijing, 2001.
11. Guinier, A.; Fournet, G. Small-Angle Scattering of X-Rays; Wiley: New York, 1955.
12. Wu, T. W.; Speapen, F. Acta Metall 1985, 33, 2185.
13. Porod, G. Kolloid-Z 1951, 124, 83.
14. Porod, G. Kolloid-Z 1952, 125, 51.
15. Meng, Z. F. Acta Sci Naturalium Univ Jilin 1989, 3, 67.
16. Strobl, G. R.; Schneider, M. J Polym Sci, Polym Phys Ed 1980, 18, 1343.
17. Debye, P.; Bueche, A. J Appl Phys 1949, 20, 518.
18. Buchanan, D. R.; McCullough, R. L.; Miller, R. L. Acta Crystallogr 1968, 20, 922.
19. Mandelkern, L.; Alamo, R. G.; Kennedy, M. A. Macromolecules 1990, 23, 4721.
20. Zhang, H. F.; Yang, B. Q.; Zhang, L. H.; Mo, Z. S. Macromol Chem Phys 1996, 197, 553.
21. Könke, U.; Zachmann, H. G.; Baltá-Calleja, F. J. Macromolecules 1996, 29, 6019.